Planetary and Space Science 57 (2009) 725–734

Contents lists available at ScienceDirect

Planetary and Space Science

journal homepage: www.elsevier.com/locate/pss

The scientific rationale for the C1XS X-ray spectrometer on India's Chandrayaan-1 mission to the moon

I.A. Crawford [a,*], K.H. Joy [a,b,c], B.J. Kellett [b], M. Grande [d], M. Anand [c,e], N. Bhandari [f], A.C. Cook [d], L. d'Uston [g], V.A. Fernandes [h], O. Gasnault [g], J. Goswami [f], C.J. Howe [b], J. Huovelin [i], D. Koschny [j], D.J. Lawrence [k], B.J. Maddison [b], S. Maurice [g], S. Narendranath [l], C. Pieters [m], T. Okada [n], D.A. Rothery [e], S.S. Russell [c], P. Sreekumar [l], B. Swinyard [b], M. Wieczorek [o], M. Wilding [d]

[a] Centre for Planetary Sciences, Birkbeck/UCL Research School of Earth Sciences, Gower Street, London WC1E 6BT, UK
[b] Space Science and Technology Department, Rutherford Appleton Laboratory, Didcot, Oxon OX11 0QX, UK
[c] Department of Mineralogy, Natural History Museum, Cromwell Road, London SW7 5BD, UK
[d] Institute of Mathematical and Physical Sciences, University of Wales, Aberystwyth, Ceredigion SY23 3BZ, UK
[e] Department of Earth and Environmental Sciences, Open University, Milton Keynes MK7 6AA, UK
[f] Physical Research Laboratory, Navrangpura, Ahmedabad 380009, India
[g] Centre d'Etude Spatiale des Rayonnements, CNRS/UPS, Toulouse, France
[h] Berkeley Geochronology Center, Berkeley, USA
[i] Observatory, PO Box 14, FI-00014 University of Helsinki, Finland
[j] European Space Agency, ESTEC, The Netherlands
[k] Applied Physics Laboratory, Johns Hopkins University, USA
[l] Indian Space Research Organisation, Bangalore, India
[m] Brown University, RI, USA
[n] Institute of Space and Astronautical Science, Japan Aerospace Exploration Agency, Sagamihara, Kanagawa 229-8510, Japan
[o] Institut de Physique du Globe de Paris, France

ARTICLE INFO

Article history:
Received 1 April 2008
Received in revised form
26 September 2008
Accepted 1 December 2008
Available online 24 December 2008

Keywords:
Moon
Lunar science
X-ray spectroscopy

ABSTRACT

The UK-built Chandrayaan-1 X-ray Spectrometer (C1XS) will fly as an ESA instrument on India's Chandrayaan-1 mission to the Moon, launched in October 2008. C1XS builds on experience gained with the earlier D-CIXS instrument on SMART-1, but will be a scientifically much more capable instrument. Here we describe the scientific objectives of this instrument, which include mapping the abundances of the major rock-forming elements (principally Mg, Al, Si, Ti, Ca and Fe) in the lunar crust. These data will aid in determining whether regional compositional differences (e.g., the Mg/Fe ratio) are consistent with models of lunar crustal evolution. C1XS data will also permit geochemical studies of smaller scale features, such as the ejecta blankets and central peaks of large impact craters, and individual lava flows and pyroclastic deposits. These objectives all bear on important, and currently unresolved, questions in lunar science, including the structure and evolution of any primordial magma ocean, as revealed by vertical and lateral geochemical variations in the crust, and the composition of the lunar mantle, which will further constrain theories of the Moon's origin, thermal history and internal structure.

1. Introduction

The primary scientific importance of the Moon arises from the fact that it has an extremely ancient surface, mostly older than 3 billion years, with some areas extending almost all the way back to the origin of the Moon 4.5 billion years ago. It therefore preserves a record of the early geological evolution of a terrestrial planet which more complicated bodies, such as Earth, Venus and Mars, have long lost. Theories of lunar evolution derived from petrological investigations of the Apollo and Luna samples have been greatly refined by the global geochemical and mineralogical datasets provided by the Clementine and Lunar Prospector missions combined with studies of lunar meteorites (see Jolliff et al., 2006, for a review). In particular, the heterogeneous nature of the lunar crust, and the dichotomy between nearside and farside crustal geochemistry (e.g., Jolliff et al., 2000; Korotev, 2005; Shearer et al., 2006; Taylor et al., 2006) show that the highland crust is more complex than expected from simplistic early models of plagioclase floatation in a global magma ocean (Taylor, 1982, 1989). This has necessitated a re-examination of lunar geological history and upcoming missions to the Moon provide a new opportunity for mapping the compositional

* Corresponding author. Tel.: +44 207 679 3431; fax: +44 207 679 2867.
E-mail address: i.crawford@ucl.ac.uk (I.A. Crawford).

0032-0633/$ - see front matter © 2008 Elsevier Ltd. All rights reserved.
doi:10.1016/j.pss.2008.12.006

diversity of the lunar surface in greater detail. Here we describe the scientific objectives of one such instrument: the Chandrayaan-1 X-ray spectrometer (C1XS) that was launched on 22 October 2008 on India's first mission to the Moon.

2. A brief history of lunar X-ray spectroscopy

X-ray fluorescence (XRF) spectroscopy provides an opportunity to map planetary surfaces in low-energy X-rays, including the characteristic signatures of the main rock-forming elements (see Yin et al., 1993, for a review). The Sun is the main source of lunar X-ray excitation and typical levels of solar intensity will result in the excitation of low atomic number elements, including Mg, Al and Si. In periods of intense activity (i.e., solar flares) X-ray lines for additional elements (e.g., Fe, Ti, Ca, P, Na, K, Mn and Co), may also be detected. Incident solar X-rays only penetrate into the upper few micrometers, or at most a few tens of micrometers (depending on the energy and the nature of the surface), producing fluorescent X-rays from the upper regolith environment (Clark and Trombka, 1997). Lunar X-ray fluorescence (XRF) was first successfully detected by the Russian Luna 12 mission in 1968 (Mandel'Shtam et al., 1968). The Apollo 15 and 16 XRF experiments were the first attempt to conduct compositional X-ray spectrometry on a planetary scale, where a simple proportional counter instrument measured the X-ray photon count-rate from the lunar surface. Data were presented as intensity ratios of Al/Si and Mg/Si as Si varies little (no more than ~5%) in lunar regoliths (Adler et al., 1973; Yin et al., 1993). These datasets provided an initial understanding of the variable geochemistry of the lunar surface, paving the way for a new generation of lunar X-ray spectrometers. These include the D-CIXS instrument on SMART-1 (see below), and more recently X-ray spectrometers on the Japanese Kaguya (Shirai et al., 2008; Okada et al., 2008) and Chinese Chang'e-1 lunar orbiters. The technique has also been used to study the surface composition of near-Earth asteroids [i.e., by NASA's NEAR mission to 433 Eros (Nittler et al., 2001) and JAXA's Hayabusa mission to 25143 Itokawa (Okada et al., 2006)], and will be employed by forthcoming missions to Mercury [i.e., NASA's MESSENGER mission (Schlemm et al., 2007) and ESA's BepiColombo (Fraser et al., 2008)]. These instruments either used gas-filled proportional counters (Apollo, NEAR, MESSENGER), or solid-state (CCD or active pixel sensor) technology (Hayabusa, Kaguya, Chang'e-1, BepiColombo), for X-ray detection.

The UK flew a demonstration version of a compact imaging X-ray spectrometer (D-CIXS) on the European Space Agency's SMART-1 mission to the Moon between 2003 and 2006 (Grande et al., 2003, 2007). This instrument demonstrated a new approach to building miniaturized X-ray detector technology, based around the use of innovative swept charge device (SCD) solid-state detectors (Holland et al., 2004). While successfully demonstrating the technology, the scientific results from D-CIXS (Grande et al., 2007; Joy, 2007; Swinyard et al., 2008), were limited by (i) the large and variable lunar footprint resulting from SMART-1's high, elliptical orbit (~300×3000 km); (ii) the low solar flare state during the mission; (iii) radiation damage to the detectors during the long (15 month) journey to the Moon and (iv) a number of unanticipated instrument and calibration problems (Joy, 2007; Grande et al., 2007).

3. Summary of the C1XS instrument

The C1XS instrument and its calibration is described in detail in the accompanying papers by Grande et al. (2008), Howe et al. (2008a) and Kellett et al. (2008). It builds on the technology inherited from D-CIXS, but will be a scientifically much more capable instrument. In order to derive elemental abundances from fluorescent X-ray data it is necessary to measure the illuminating solar X-ray spectrum, and this will be provided by an accompanying X-ray solar monitor (XSM), which is also similar to that developed for SMART-1 (Alha et al., 2008).

Specific areas where C1XS will improve on the performance of D-CIXS are as follows.

3.1. Instrumental and hardware improvements

Operating D-CIXS during the lunar phase of the SMART-1 mission highlighted a number of problems with the instrument which have been corrected for C1XS (see Howe et al., 2008a for details). One of the most serious problems with D-CIXS was that the spectra occasionally exhibited double peaks (i.e., the same spectral line would occur at two energies some 100's of eV apart); these spectra had to be discarded. Following further development using the D-CIXS engineering model it was shown that synchronising the SCD readout to the SCD power supply eliminated this double-peaking effect and this improvement has been implemented on C1XS.

Development work on the prototype C1XS instrument also showed that improving the X-ray event detection algorithm was essential, this was achieved using two detection thresholds within a field programmable gate array (Howe et al., 2008a). The other significant change was to the video processing strategy. The earlier D-CIXS instrument measured the zero energy level and then adjusted a hardware offset to make the zero energy match the analogue to digital converter (ADC) zero value. However, due to the coarse offset adjustment this was never very effective. The strategy for C1XS is to position the zero energy level within the range of the ADC (around channel 400 out of 16384) such that it stays within the ADC scale for the range of expected SCD operating temperatures; C1XS then transmits both the X-ray data and samples of the "zero" data, so that the energy zero position is well known.

Finally, it was also observed that D-CIXS ran much hotter than intended. As a consequence the thermal design of C1XS was completely re-worked and a dedicated radiator has been provided to cool the X-ray detectors to ensure that their temperature is less than $-17\,^{\circ}$C.

3.2. Spatial resolution

The C1XS collimator stack (described in detail in Section 2.1 of Howe et al., 2008a) permits X-rays from a 28°-wide aperture (i.e., $\pm 14^{\circ}$) to fall on each SCD detector, corresponding to 50 km on the lunar surface from Chandrayaan's circular 100 km orbit. The corresponding value for D-CIXS ranged from 63 to 630 km as SMART-1 executed its elliptical orbit around the Moon. The uniform spatial resolution of C1XS will greatly simplify the data analysis, as well as ensuring that all lunar terrains are covered with sufficient resolution to address the key scientific objectives outlined below. We note that the sensitivity of each SCD will be weighted towards the centre of its field of view, and thus towards the central 14° of the collimator aperture, corresponding to 25 km on the lunar surface. This defines the full-width at half-maximum (FWHM) of the collimator's transmission function. Fig. 1 shows the full 50 km footprint, and the central 25 km, superimposed on the central peak of the large farside crater Tsiolkovsky, which shows that features of this size will be resolvable. Depending on the signal-to-noise ratio (SNR) achieved, the transmission function may in principle be de-convolved from the data to reveal geochemical information on scales $\leqslant 25$ km; Fig. 2 illustrates this

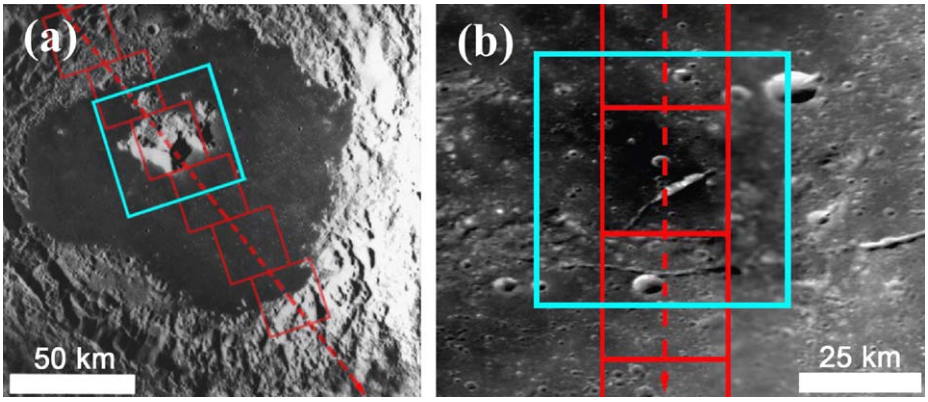

Fig. 1. Illustration of C1XS spatial resolution, superimposed on (a) the central peak of the large farside mare-filled crater Tsiolkovsky, and (b) a presumed pyroclastic deposit surrounding an endogenic crater on the floor of the eastern Mare Frigoris (34.45°, 50.17°). In each diagram the blue box represents full spatial footprint of 50 km, the red boxes sequential positions of the 25 km FWHM PSF and the red dashed line represents the spacecraft ground track; note that these are instantaneous footprints: for a nominal 8 second integration time orbital motion will stretch the PSF along the track by an additional 13 km (images courtesy of NASA/LPI). (For interpretation of the references to colour in this figure legend, the reader is referred to the web version of this article.)

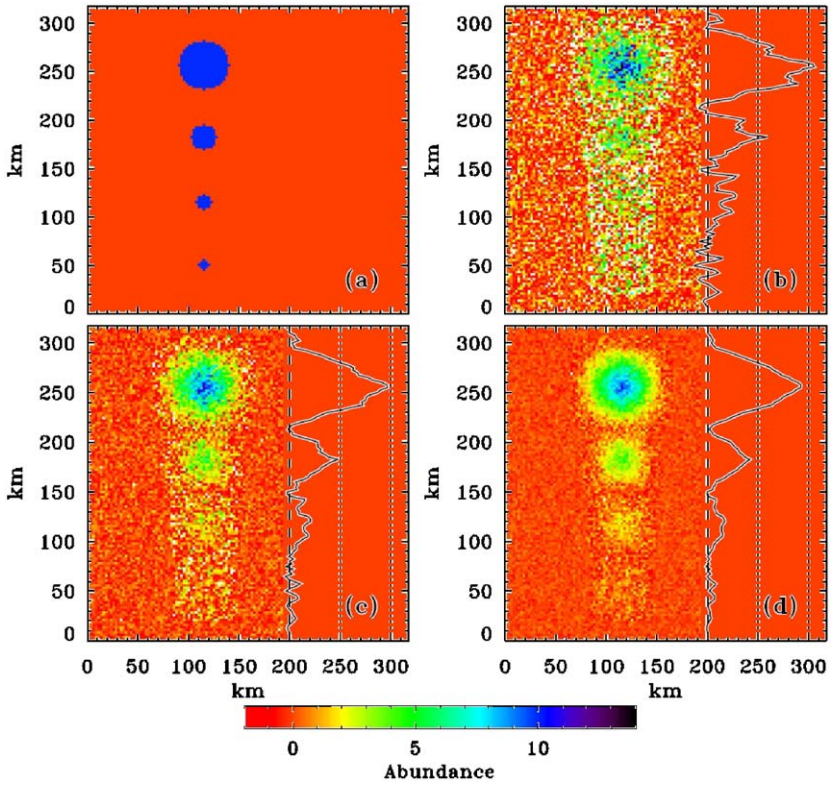

Fig. 2. Illustration of C1XS spatial resolution. (a) Idealised input for an element that has zero abundance everywhere except for circular features which are composed of a uniform 10 elemental wt%. The sizes of these features are 10, 15, 25 and 50 km diameter (bottom to top). The other panels show the result of convolving this idealised input with the C1XS collimator response for signal-to-noise ratios and background levels expected in the region of the low-energy lines (i.e., Mg, Al and Si) for: (b) a C5-class flare; (c) an M1 flare; and (d) an M5 flare. In these panels the solid line shows the intensity through the centre of the features with the dashed line representing 0 wt% and the two dotted lines indicating 5 and 10 wt%. Note that for M-class flares or higher sub-25 km scale structure is in principle resolvable given a sufficient abundance contrast.

possibility and shows that features as small as ~15 km with high elemental contrast should be detectable.

3.3. Spectral resolution

The C1XS science requirements document (Maddison et al., 2006) specifies an energy resolution of <180 eV FWHM (at 1.49 keV), primarily to ensure adequate resolution of the closely spaced Kα lines of Mg (1.25 keV), Al (1.49 keV) and Si (1.74 keV), which are of high scientific priority. Laboratory testing of the C1XS flight instrument has demonstrated an energy resolution of ⩽110 eV at Al Kα, which may be compared with the ~360 eV resolution of D-CIXS. The low-energy resolution of D-CIXS (Grande et al., 2007), which essentially made it impossible to resolve the Mg, Al and Si lines, was due in part to radiation damage incurred during SMART-1's 15-month journey to the Moon, but this will not be so much of an issue with the much shorter (~16 day) flight of Chandrayaan-1 (although radiation-induced degradation of several tens of eV is still possible; Howe et al., 2008b). Detection of the Mg line was further compromised for D-CIXS because of blending with the poorly characterised low-energy noise peak

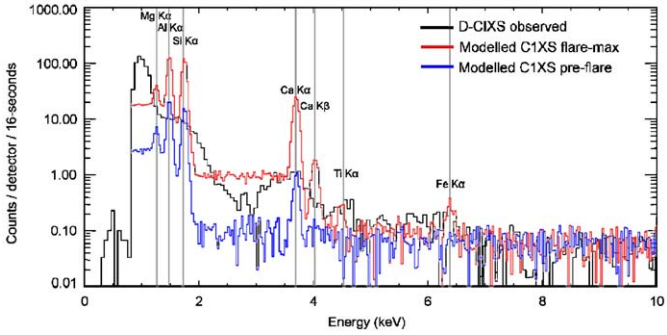

Fig. 3. Comparison between an actual D-CIXS spectrum, obtained on November 18 2005 over a mixed mare/highland region in the vicinity of Mare Cognitum (Swinyard et al., 2008), and the predicted C1XS performance for the same solar flare event assuming an Apollo 11 soil composition (to which the D-CIXS results approximate; see Swinyard et al., 2008 for details). The C1XS energy resolution (FWHM = 110 eV) adopted was that obtained with an Al-anode during calibration of the flight instrument in the Rutherford Appleton Laboratory's RESIK facility (Narendranath et al., 2008; Kellett et al., 2008), assuming the co-registration and addition of all 24 SCD detectors. The red spectrum shows the modelled C1XS response during the peak of this M1 class flare, while the blue spectrum shows the modelled response for the quiescent period before the flare began. It is clear that, even in the latter case, the Mg, Al, Si and Ca Kα lines will be detectable, and fully resolvable with C1XS, which was not the case with D-CIXS. At the M1 flare level, Ti and Fe will be clearly detected. (For interpretation of the references to colour in this figure legend, the reader is referred to the web version of this article.)

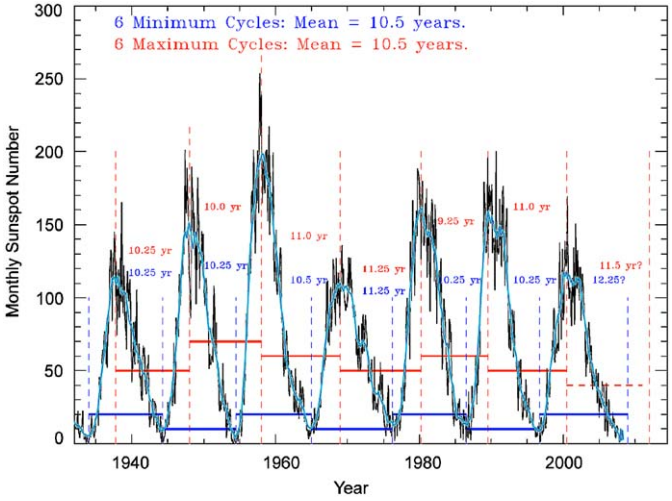

Fig. 4. The raw and smoothed behaviour of sun spot number (SSN) for the last seven solar cycles. The average min–min and max–max periods for the 6 completed cycles shown are both 10.5 years. However, the last cycle (cycle 23) is already over 12 years in extent (measured for the previous minimum).

(Grande et al., 2007). As described in Section 3.1 above, instrumental improvements have now ensured that this will not occur with C1XS (see also Howe et al., 2008a).

Fig. 3 shows a comparison between an actual D-CIXS spectrum, obtained on November 18 2005 over a mixed mare/highland region in the vicinity of Mare Cognitum (Swinyard et al., 2008), and the predicted C1XS performance for the same solar flare event assuming an Apollo 11 soil composition (to which the D-CIXS results approximate; see Swinyard et al., 2008 for details). The incident solar X-ray flux was taken from the Geostationary Operational Environmental Satellite (GOES) database (http://rsd.gsfc.nasa.gov/goes/; see also Hanser and Sellers, 1996). For convenience, we adopt the GOES classification of solar flare intensities, where the letters B, C, M and X designate bands of increasing X-ray luminosity, with an increase by a factor of 10 between each band. Two calculations have been performed: once for the peak of this M1 class flare (red spectrum in Fig. 3) and once for the quiescent (C-level) period before the flare began (blue spectrum in Fig. 3). It is clear that, even in the latter case, the Mg, Al, Si and Ca Kα lines will be detectable, and fully resolvable with C1XS, which was not the case with D-CIXS. At the M1 level, Ti (only marginally detected in the D-CIXS spectrum; Swinyard et al., 2008) and Fe (not detected at all in the D-CIXS spectrum) will be clearly detected.

3.4. Enhanced solar X-ray flux

D-CIXS operated close to solar minimum (at the end of Solar Cycle 23), and too few sufficiently strong (i.e., C3 class or higher) solar flare events occurred during the SMART-1 mission for many meaningful fluorescence spectra to be obtained from the lunar surface (Joy, 2007; Grande et al., 2007; Swinyard et al., 2008). Chandrayaan-1 will fly during the rise to the next solar maximum (Cycle 24) and higher X-ray fluxes may be expected, although this clearly depends on exactly when the next cycle begins and the duration of the mission.

The recent behaviour of the Sun can be seen in Fig. 4 which focuses on the last 80 years. Measuring the cycle length from minimum to minimum or maximum to maximum actually gives very similar results—the last 6 completed cycles have an average duration of 10.5 years. However, Fig. 4 indicates that the current cycle (23) was in operation well into 2008. This means that the current solar minimum is still to come, and that the current minimum–minimum cycle length is therefore in excess of 12 years—making the current cycle the longest one for around 100 years. Chandrayaan-1 was launched in October 2008. In other words, the launch occurred almost exactly at the end of cycle 23 and the beginning of cycle 24. This means that we can now perform simulations of the C1XS X-ray coverage of the lunar surface based on a firm understanding of solar cycle phase.

The "true" solar cycle length is actually twice the observed cycle because it is a magnetic phenomenon that underlies solar activity. That is, to get to the same magnetic phase of the solar activity cycle we need to go back two cycles. Thus, in the first instance, we should use the X-ray behaviour of the Sun from Cycle 22 which started around 1986.5 to try and simulate the likely C1XS mapping coverage of the Moon. We have therefore taken the observed GOES X-ray flux of the Sun measured at 1 min intervals and folded these in with a simulation of Chandrayaan-1 orbiting the Moon. The simulation is somewhat simplified in that the orbit is assumed to be fixed/circular and no account is taken of phase angle. The simulation does, however, take account of whether Chandrayaan-1 is on the sunlight or dark hemisphere of the Moon—C1XS can only observe X-ray flares that fall on the sunlight hemisphere (i.e., only ~50% of all solar flares can ever be seen by a satellite in a polar/circular orbit around the Moon). The simulations divide the Moon into 25 km squares and each of these 25 km pixels is flagged according to the flare state measured in the GOES data for Cycle 22. At the end of each lunar rotation, C1XS will have viewed the entire lunar surface in sunlit conditions and the percentage of pixels at C, M and X levels can be calculated.

The results of these simulations are shown in Fig. 5 and Table 1. The simulations were done for three possible launch dates—absolute solar minimum and then three and six months later (actually 90 and 180 days later). These start dates are indicated by the dashed and dash–dot lines close to the beginning of the plot. The nominal 25 lunar rotations (2-year) mission end points are indicated by the same line type at the end of the plot (the dotted line indicating where the end of the absolute minimum simulation occurs). The C, M and X flare coverage percentages are shown by the blue, green and red lines. In all three cases these lines

converge for the three different start times. This shows that the much higher level of activity in the later lunar rotations is more than sufficient to "fill in" the gaps missed earlier in the mission. The conclusion is very clear, the later C1XS starts survey the Moon in Cycle 24 the quicker it will be able to cover the Moon in C flare conditions, and the more of the Moon will be covered in the M and X flare maps. These flares are the ones that will allow C1XS to map the less abundant or harder to excite elements—such as titanium and iron. The black line on Fig. 5 shows the "4 × C" percentage. This is the percentage of the Moon that receives 4 different C flares. These pixels will also provide "better" results in the final analysis either because of the greater flux or because of the occurrence of flares with different phase angles.

The results indicate that if Chandrayan-1 were to commence operations six months after solar minimum (which now seems unlikely), and the Sun achieves a similar level of flare activity in Cycle 24 as seen in Cycle 22, then we should achieve our baseline objectives within the nominal 2 year (25 lunar rotation) mission duration. Otherwise, a six month to a year extension in mission lifetime will be required. Such an extension is in any case desirable as it would yield significant gains in the percentage of M and X flare coverage.

3.5. Increased accuracy in key elemental abundance and elemental ratio determinations

The modelled performance of the instrument (see Fig. 3 above) indicates that flare states of C1 or higher will permit good detections of Mg, Al and Si; C4 states or higher will permit good detections of Ca; while M-class flares will be required for good measurements of Fe and Ti (wherever their concentrations are greater than about 1 wt%). We quantify this in Table 2, which shows the signal-to-noise ratio estimates for the key element lines as a function of flare state (assuming a surface composition equal to that of soils returned from the Apollo 16 landing site, a 16 s integration, and co-adding all 24 detectors; see Swinyard et al., 2008).

Table 1 indicates that, even for a launch at solar minimum, >80% of the lunar surface will be observed at C1 level or higher during the nominal 2-year mission, enabling essentially all the science objectives relying on Mg, Al and Si measurements to be met. Magnesium, in particular, is a key element for the C1XS science objectives, and the C1XS science requirements (Maddison et al., 2006; Joy et al., 2008) specify that the Mg/Si ratio should be measurable to 10% (3σ) for C-class flares or above, and our performance predictions indicate that these requirements should easily be met. Fig. 6 indicates that 10% errors in these (low-energy) elemental ratios are sufficient to distinguish between different lunar lithologies.

High SNR spatial coverage for Fe and Ti will inevitably be lower (probably <10% for the nominal mission, rising to >30% given a 12-month extension), but this will still be sufficient to achieve many of the science objectives specified below. The Ti measurements will be particularly useful for the remote mapping and classification of mare basalts (see below), while even 10% coverage for Fe will permit direct measurements of the important Mg/Fe ratio, at least on regional scales.

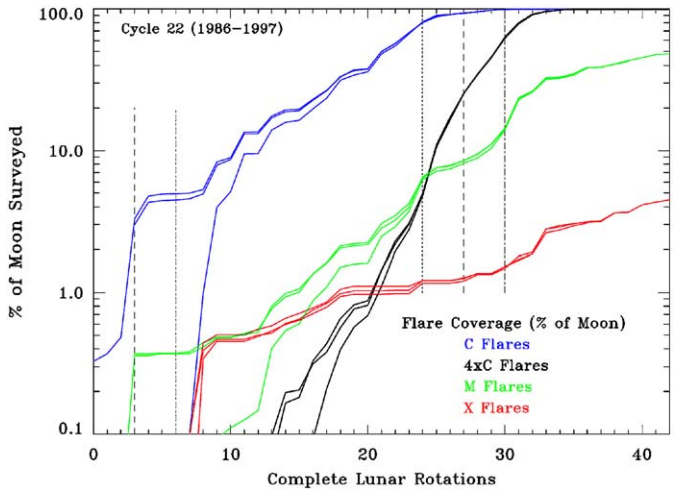

Fig. 5. The prediction of the mapping performance of C1XS based on real GOES measured X-ray fluxes for cycle 22 (see text for details).

Table 2
Estimated signal-to-noise ratios for key elemental lines as a function of flare state given elemental concentrations as measured at the Apollo 16 site (Mg: 3.6 wt%; Al: 14.4 wt%; Si: 21.0 wt%; Ca: 10.4 wt%; Ti: 0.32 wt%; Fe: 3.9 wt%; Haskin and Warren, 1991).

Line	Flare state			
	B1	C1	C4	M1
Mg Kα	~10	>100	>100	>100
Al Kα	>100	>100	>100	>100
Si Kα	>100	>100	>100	>100
Ca Kα	<5	~25	~80	>100
Ti Kα	ND	ND	ND	~12
Fe Kα	ND	ND	ND	~16

Estimates assume a 16 s integration and the co-addition of all 24 SCD detectors. Noise was estimated from the standard deviation of the flat parts of the background close to the lines; the line flux has here been taken to be the peak flux, which is conservative. In reality the line flux will be obtained by fitting the known response function. Any SNR>100 will in practice be dominated by non-statistical noise sources (e.g., calibration errors, etc.) and so is here marked simply as >100; ND indicates that a line is not detected. Note that, as Apollo 16 sampled a highland site, these numbers are conservative with regard to the detectability of Mg, Ti and Fe.

Table 1
Percentage of the lunar surface covered by flares of different X-ray magnitude for the mission durations shown in the left hand column (expressed as the number of lunar rotations).

Mission duration (lunar rot.)	C flare level			4 × C flare level			M flare level			X flare level		
	Min	Min+3	Min+6	Min	Min+3	Min+6	Min	Min+3	Min+6	Min	Min+3	Min+6
12	13.5	18.8	23.5	0.0	0.2	0.2	0.5	1.0	1.1	0.50	0.60	0.79
25	80.2	93.6	99.7	4.9	25.3	63.6	6.4	8.5	14.0	1.21	1.27	1.48
31	99.5	100	100	62.3	96.4	99.9	14.2	33.5	38.5	1.52	2.79	3.14
36	100	100	100	99.8	100	100	38.9	42.6	48.3	3.08	3.67	4.49

The simulations are based on actual flare statistics for Cycle 22 and were performed for three different launch scenarios—launch exactly at solar minimum and then +3 and +6 months later. The "4 × C" column gives the fraction of the surface covered by 4 separate C-class flares within the specified mission duration.

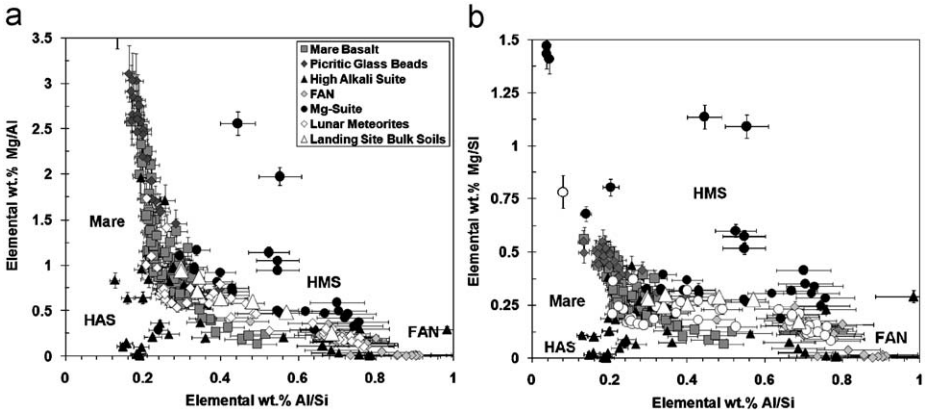

Fig. 6. A number of different lunar lithologies (see key at top; FAN: ferroan anorthosite; HMS: high Mg suite; HAS: high alkali suite) shown on plots of Mg/Al vs. Al/Si (left) and Mg/Si vs. Al/Si (right). Data collated from BVSP (1981), Papike et al. (1998), Warren (2005), Korotev (2005) and Wieczorek et al. (2006). The error bars indicate 10% errors on these elemental ratios and the major lithological groupings are still resolvable given this level of precision; C1XS will aim to achieve this level of precision or better.

Taken together, these significant improvements over D-CIXS mean that C1XS is uniquely placed to address a number of key lunar science objectives.

4. C1XS science objectives

To a large extent the scientific objectives of C1XS mirror those identified for D-CIXS (see Dunkin et al., 2003), but the greater spatial and spectral resolutions anticipated for C1XS mean that it will be possible to address more specific science goals than were identified for the former instrument. Ultimately, all of these science objectives bear on important questions of lunar crustal and mantle evolution, and will provide further insights into our understanding of the origin of the Moon. For the sake of the subsequent discussion, we divide the science objectives into "regional" and "local" studies. The former will be addressable with the ~50 km/pixel resolution which corresponds to the full footprint of the 28° collimator field of view, while the latter will require spatial resolutions of $\leqslant$25 km and therefore possibly require some deconvolution of the 25 km FWHM of the instrumental transfer function.

4.1. Regional studies

4.1.1. Major element geochemistry of major lunar terrains

A major objective of C1XS is to map the abundances of the major rock-forming elements (principally Mg, Al, Si, Ca and, for high flare states, Ti and Fe) in the lunar crust, and especially in so-far unsampled regions. Jolliff et al. (2000) identified three major lunar terrains: the Procellarum KREEP Terrain (PKT) on the NW–central nearside; the Feldspathic Highlands Terrain (FHT), which largely comprises the farside highlands; and the South Pole-Aitken Basin (SPA). Compositional differences between these major crustal terrains are key to understanding their origin, and thus early lunar crustal and mantle evolution (Jolliff et al., 2000; Shearer and Floss, 2000; Shearer et al., 2006). However, to-date only localities within or adjacent to the PKT have been sampled *in situ*, and studies of the other two terrains must rely on remote sensing methods and statistical arguments based on the petrology and geochronology of lunar meteorites (Korotev, 2005 and references cited therein; Warren, 2005). As discussed below, observations of regional variations in Mg will be especially useful in constraining theories for the origin and evolution of these terrains.

4.1.2. Orbital determination of Mg#

One particularly important area where C1XS has the potential to make significant advances is through the determination of the Mg abundance, or more specifically the Mg number (Mg# = atomic Mg/(Mg+Fe)), in the lunar surface. Owing to the different compatibilities of Mg and Fe in the primary rock-forming minerals, Mg# is an important parameter for distinguishing between different lunar lithologies and evolutionary models (e.g., Lucey et al., 2004; Cahill et al., 2005). Typically, Mg# of mafic mineral phases, or the bulk sample, provides an indication of petrological "evolutionary state", with the most primitive minerals/rocks having high Mg#, and most evolved minerals/rocks having a low Mg#. In fact, there are at least three different aspects of lunar science that would benefit from high-resolution determinations of Mg#:

(i) maps of Mg# will help constrain the regional distribution of the Mg suite of rocks, about which different models of crustal evolution make different predictions. In particular, they will allow us to determine whether, as is sometimes argued, the Mg suite is petrogenetically related to the KREEP-rich lithologies (e.g., Snyder et al., 1995), and therefore restricted to within the PKT, or whether the farside FHT also has a high-Mg component that may have similar intrusive origins to those inferred for the nearside magnesian suite but without a KREEP component (Wieczorek et al., 2006; Shearer et al., 2006 and references cited therein);
(ii) different models of lunar crustal evolution also predict different variations of Mg# as a function of depth into the crust (e.g., Jolliff, 2006), so measurements of Mg# from different stratigraphic levels within the crust will help discriminate between these models; and
(iii) measurements of the Mg# of basaltic lava flows may provide information of the Mg# of the mantle sources of their parental magma, and/or the degrees of partial melting of these sources (and subsequent fractionation history). This may help constrain the bulk Mg# of the lunar mantle as a whole, which has implications for theories of lunar origin (Warren, 1986).

Although attempts have been made to map Mg# using Clementine multi-spectral and Lunar Prospector gamma-ray data (Fig. 7; see also Cahill et al., 2005; Prettyman et al., 2006), these maps lack the precision and the spatial resolution required to make significant inroads into the above questions (although Fig. 7

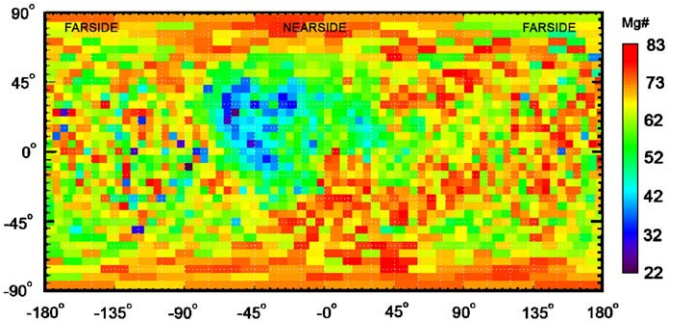

Fig. 7. Global Mg# variations as derived from the Prettyman et al. (2006) two degree MgO and FeO Lunar Prospector dataset.

already suggests that there is some variability in Mg# within the highlands, with average values higher around 100°E than around 100°W, for example). The high spatial resolution of C1XS ($\leqslant$50 km), coupled with the spectral resolution ($<$180 eV) required to unambiguously resolve the 1.25 keV Mg Kα line from the adjacent 1.49 keV Al line (Fig. 3), will enable sufficiently precise Mg concentrations to be obtained for most of the lunar surface for the first time. In order to obtain self-consistent maps of Mg# it is also desirable to make simultaneous observations of Fe with the same footprint. With C1XS this may only be possible for the ~10% of the time when the solar X-ray illumination is sufficient (M5 or higher) to excite detectable Fe fluorescence. However, this 10% coverage will be sufficient to correlate the C1XS Fe abundances with those obtained by Clementine and Lunar Prospector, allowing those data sets to be reliably combined with the C1XS Mg measurements to yield near global coverage of Mg# at $<$50 km resolution.

4.1.3. *Refractory element budget of lunar crust*

C1XS will be able to detect the variability of the concentration of Ca and Al in the lunar crust. These elements are important for our understanding of the refractory element budget of the bulk Moon and how this budget compares to the Earth and other terrestrial planets. There are divergent theories as to the refractory budget of the Moon (Taylor, 1980, 2007; Warren and Rassmusen, 1987; Longhi, 2006; Taylor et al., 2006). Warren and Rassmusen (1987) and Longhi (2006) argued that the bulk Moon has a similar or slightly depleted Al-content to the Earth (Moon/Earth is 1 or just $<$1), whilst Taylor et al. (2006) argue that the bulk Al-budget of the Moon is much greater than the Earth (i.e., Moon/Earth is $>$1.5). C1XS will be able to provide the first accurate global measurement of the concentration of Al_2O_3 (and CaO) in the lunar crust, helping to better constrain some of the key parameters needed to successfully geochemically model the composition of the lunar crust, and through it the Moon as a whole. Understanding this geochemistry will allow constraints to be made in understanding lunar magma ocean thickness, differentiation (including the efficiency of plagioclase flotation during crystallisation), duration and heterogeneity.

4.1.4. *Large-scale stratigraphy of the lower crust*

Determination of the geochemistry of the lunar crust as a function of depth in different regions of the Moon greatly aids our understanding of the stratigraphy of the lunar crust. C1XS will contribute to this aspect of lunar science by measuring the abundances of the major rock-forming elements in the floor of large basins not obscured by mare basalts (including SPA and other farside basins), and the central rings and/or ejecta blankets of impact basins (whether flooded or not) which expose material derived from depths of many tens of km (Spudis, 1993). The extent to which the mafic component of the (seemingly noritic) lower crust is relatively magnesian or ferroan in composition is uncertain, yet has significant implications for our understanding of crustal formation through plagioclase flotation in an early magma ocean (e.g., Wieczorek and Zuber, 2001; Jolliff, 2006; Shearer et al., 2006 and references cited therein). In the special case of SPA, where most of the upper crust is likely to have been removed, observations of the geochemistry and Mg# of the (as-yet unsampled) floor material will probe the deepest stratigraphic levels of the lunar crust to which we have access, and may possibly reveal outcrops of lunar mantle material (e.g., Pieters et al., 2001). We note that finding outcrops of lower crustal and/or mantle composition through orbital remote sensing will be of potential interest for future sample return missions, as they can then be targeted so as to shed maximum light on lunar stratification and differentiation.

4.1.5. *Mare basalt composition and evolution*

C1XS will enable a number of studies of lunar lava flows, which will further inform our knowledge of the thermal and chemical evolution of the lunar mantle. For example, observations of the composition of farside maria (e.g., Mare Moscoviense) will enable a comparison with nearside mare compositions and allow us to determine whether they have arisen from geochemically similar mantle source regions, and whether they are more enriched in Al owing to crustal assimilation due to the thicker farside crust. C1XS will also permit a comparison of major element geochemistry of stratigraphically distinct large-scale lava flows in the same geographical region (e.g., Oceanus Procellarum, Imbrium Basin, etc.) to study mantle evolution with time in specific regions. For example, northern Oceanus Procellarum consists of a patchwork of discrete lava flows with estimated individual ages ranging from about 3.5 to 1.2 Gyr (Wilhelms, 1987; Hiesinger et al., 2003). Determining how the compositions of these lava flows have changed with time would yield insights into the thermal and magmatic evolution of the lunar mantle and assist in the construction of a more complete stratigraphy of the maria. The anticipated sensitivity of C1XS to Ti (see Section 3.3 above) will be particularly useful in this regard as Ti content is one of the primary diagnostics of mare basalt petrogenesis (Neal and Taylor, 1992), but existing global Ti maps are not in good agreement (e.g., Prettyman et al., 2006). There is also some disagreement regarding the Fe abundance of some unsampled mare basalts (e.g., in western Procellarum), where Clementine and Lunar Prospector results are in disagreement (Lawrence et al., 2002) and C1XS data may help resolve this discrepancy.

C1XS will also permit compositional studies of basaltic lavas that pre-date the mare basalts represented in the sample collection, which would be especially valuable for constraining models of lunar crustal and mantle evolution. For example, it will be possible to conduct a search for outcrops of the high-Al basalts. Currently these are only identified as clasts within breccias returned by the Apollo 12, 14 and Luna 16 missions, and are thought to represent some of the earliest phases of lunar volcanism (e.g., Kramer et al., 2004). Similarly, C1XS will enable detailed compositional studies of as-yet unsampled outcrops of other presumed pre-mare basalts, such as the KREEP basalts that are probably exposed on the Apennine Bench Formation in south-eastern Mare Imbrium. The geochemistry of these basalts, and especially their Mg#, should help elucidate the nature of the hypothesised ur-KREEP layer at the base of the crust in this region of the Moon, and its role in the evolution of the PKT (see Wieczorek et al., 2006 and references cited therein).

4.2. Local studies

4.2.1. Probing the stratigraphy of the upper-middle lunar crust

The composition of the crust to depths of up to several tens of km can be probed by determining the major element geochemistry of the central peaks and/or ejecta blankets of impact craters in the diameter range ~100–300 km. Such craters will have excavated crustal materials from depths of 10–30 km, respectively (e.g., Melosh, 1989), and materials from just below these depths will be exposed in the re-bounded central peaks. Tompkins and Pieters (1999) pioneered this technique as applied to Clementine mineralogy data, but no previous X-ray spectrometer has had sufficient spatial resolution to apply it to elemental abundances. C1XS thus has a unique opportunity to determine the vertical composition of the lunar crust from crater ejecta deposits and central peaks (Fig. 1a). There are approximately 200 lunar craters larger than about 100 km in diameter which would be suitable for investigations of this kind, and the flare statistics given in Table 2 indicate that data for at least Mg, Al and Si should be obtained for most of these within the first two years of operation. Although direct Fe measurements are more difficult, and will depend on the serendipitous occurrence of an M-class flare while C1XS is above an appropriate crater, Fe/Mg ratios can still be determined by combining C1XS Mg data with Fe concentrations obtained by previous missions (e.g., Clementine and Lunar Prospector). Note that while the resolution of the central peaks of most craters in this size range will probably require deconvolution of the instrument's 25 km transmission function (Fig. 2), resolution of the ~50 km wide continuous ejecta blankets should be more straightforward.

Craters larger than a few tens of km in mare regions may expose underlying pre-mare materials. An interesting example in this category is provided by the craters Peirce ($D = 18$ km) and Picard ($D = 22$ km) in Mare Crisium which, given geophysical indications of low crustal thickness under Crisium (Wieczorek and Phillips, 1998), may have exposed mantle materials. Indeed, Apollo orbital X-ray data revealed high levels of Mg around both these craters (Andre et al., 1978), which might be evidence for exhumed mantle. The region of elevated Mg surrounding Picard has an area of roughly 30×60 km^2 and will be resolvable by C1XS.

4.2.2. Studies of lunar cryptomaria

Cryptomaria are ancient (>3.8 Gyr) mare basalt deposits that are hidden or obscured by superposed higher albedo material, most likely basin ejecta deposits. They represent a record of the earliest mare volcanism and may be a significant volumetric contribution to the lunar crust, especially on the lunar farside. They may be identified by dark-haloed impact craters, where impact has excavated basement basaltic material (Hawke et al., 1985; Antonenko et al., 2000). Although high spatial resolution is required to resolve the relatively small dark-haloed impact craters, which may only be marginally possible with C1XS, the mixing of exhumed material from buried layers into the surface regolith by numerous small impacts may lead to larger scale compositional variations attributable to the presence of cryptomaria. C1XS observations will thus permit a search for, and geochemical characterisation of, lunar cryptomaria, which will further constrain the compositional variation of early lunar volcanic processes.

4.2.3. Geochemical characterisation of lunar pyroclastic deposits

C1XS resolution may be used to determine the major element geochemistry of presumed pyroclastic (volcanic) dark halo craters (Fig. 1b). The dark haloes are thought to be due to pyroclastic deposits of picritic glasses whose chemical composition most closely resembles that of the original mantle partial melts from which mare basalts are derived (Delano, 1986; Shearer et al., 2006 and references cited therein), and which therefore provide important windows into lunar mantle evolution. These features typically have 10–25 km scales (Head and Wilson, 1979; Hawke et al., 1989; Gaddis et al., 2000), so deconvolution of the C1XS transmission function will be required for all but the largest of them. As for the crater central peaks discussed above, there is a high probability that Mg, Al, Si (and perhaps Ca) will be obtained for a number of these features during the nominal mission, but determinations of the Fe/Mg ratio may require C1XS observations of Mg to be combined with Fe measurements from previous missions (unless an M+ class flare should occur serendipitously while the instrument is over a suitable deposit).

4.2.4. Identification of new types of lunar lithologies

The Apollo and Luna sample return missions retrieved ~382 kg of lunar rock and soil samples (Vaniman et al., 1991) from a total of nine landing sites situated in broadly equatorial areas of the lunar nearside. This dataset has provided our basic understanding of the diversity of lunar rocks. Lunar meteorites have provided an important addition to this sample collection, as they originate from previously unsampled geological settings. Lithologies that were not identified in the Apollo and Luna collection have been found in lunar meteorites (e.g., Treiman and Drake, 1983; Goodrich et al., 1985; Korotev, 2005; Takeda et al., 2006) and they are providing an important insight into the thermal (Fernandes et al., 2003; Terada et al., 2007a, b) and impact history (Fernandes et al., 2000; Gnos et al., 2004; Cohen et al., 2005) of the whole Moon. However, like the Apollo and Luna rock collections, the range of materials sampled in lunar meteorites is probably limited compared to the actual geological diversity of the Moon, and it is possible that C1XS will measure the composition of lunar regoliths that lie outside the known range of lunar rocks and soils.

4.2.5. Constraining the provenance of lunar meteorites

The orbital determinations of major element abundances obtained by C1XS will be used to help identify the regional settings from which different lunar meteorites are derived. This will permit the laboratory determinations of minor and trace elements within these samples, which cannot be determined from orbit, to be used to further constrain geochemical models of these regions of the lunar surface (see Joy et al., 2006).

4.2.6. An aid to mineralogical studies

Chandrayaan-1 will carry three instruments that are sensitive to the mineralogy of the lunar surface: the Hyperspectral Imager (HySI; Kiran Kumar and Roy Chowdhury, 2005), the Moon Mineral Mapper (M^3; Green et al., 2007), and a near infrared spectrometer (SIR2; Mall et al., 2007). Although C1XS X-ray data will not in themselves determine surface mineralogy, we can use the C1XS-derived abundances of major rock-forming elements to reconstruct normalised mineral models (e.g., CIPW-norms; Milliken and Basu, 2000). This will help in constraining mineralogical determinations made by the multi-spectral imaging and near IR spectroscopy instruments on Chandrayaan-1, and on previous and forthcoming lunar missions (e.g., Clementine, SMART-1, Kaguya and LRO). These data may enable us to resolve disagreements between chemical abundances (e.g., for Fe) as determined from Clementine reflectance spectra and those determined by the Lunar Prospector gamma-ray data (Lawrence et al., 2002). We note that mineral identifications based on elemental abundances have the advantage that they are not affected by space weathering of the surficial regolith, which can seriously affect the interpretation

of reflectance spectra (e.g., Lucey et al., 2006). Thus, C1XS data can make a significant contribution to the identification of the mineralogy of the lunar crust, despite its relatively poor spatial resolution compared to other instruments.

5. Conclusions

The UK-built C1XS X-ray spectrometer was launched as an ESA instrument on India's Chandrayaan-1 mission to the Moon in October 2008. C1XS builds on experience gained with the earlier D-CIXS instrument on SMART-1, but will be a scientifically much more capable instrument. It will be complementary to other orbital measurements of the Moon's surface elemental composition, such as multi-spectral imaging and gamma-ray spectrometry implemented on previous missions, and to the other remote sensing instruments onboard Chandrayaan-1 itself. By performing high spectral and spatial resolution measurements of the abundances of major rock-forming elements in the lunar surface, including the presently poorly constrained Mg abundance, C1XS will address important and currently unresolved questions in lunar science. These include the structure and evolution of any primordial magma ocean, as revealed by vertical and lateral geochemical variations in the crust, and the composition of the lunar mantle, which will further constrain theories of the Moon's origin, thermal history and internal structure.

Acknowledgements

We thank all the members of the C1XS technical and engineering teams at the Rutherford Appleton Laboratory, Indian Space Research Organisation, European Space Agency, University of Helsinki, Brunel University and CNRS Toulouse who have made C1XS possible. We further thank ESA for financial support and Christian Erd for his wise stewardship of the project to-date. IAC and KHJ thank the Leverhulme Trust for financial support; NB thanks the Indian National Science Academy for the Honorary Scientist grant; VAF was partially supported by PPARC/STFC, UK.

References

Adler, I., Trombka, J.I., Schmadebeck, R., Blodget, H., Eller, E., Yin, L., Lamothe, R., Osswakd, G., Gorenstein, P., Bjorkhom, P., Gursky, H., Harris, B., Arnold, J., Metzer, A., Reedy, R., 1973. Apollo 15 and Apollo 16 results of the integrated geochemical experiment. Moon 7, 487–503.

Alha, L., Huovelin, J., Hackman, T., Andersson, H., Howe, C.J., Esko, E., Väänänen, M., 2008. The in-flight performance of the X-ray solar monitor (XSM) on-board SMART-1. Nucl. Instrum. Methods Phys. Res. Sect. A 596, 317–326.

Andre, C.G., Wolfe, R.W., Adler, I., 1978. Evidence for high-magnesium subsurface basalt in Mare Crisium from orbital X-ray fluorescence data. In: Merrill, R. (Ed.), Mare Crisium: A View from Luna 24. Pergamon, New York.

Antonenko, I., Head, J.W., Mustard, J.F., Hawke, B.R., 2000. Criteria for the detection of lunar cryptomaria. Earth Moon Planets 69 (2), 141–172.

Basaltic Volcanism Study Project, 1981. Basaltic Volcanism on the Terrestrial Planets. Pergamon Press, Inc., New York, pp. 236–266 (Chapter 1.2.9, Lunar mare basalts).

Cahill, J.T., Lucey, P.G., Steutel, D., Gillis, J.J., 2005. Analysis of the lunar surface with global mineral and Mg-number maps, Lunar. Planet. Sci. Conf. 36, 2186.

Clark, P.E., Trombka, J.I., 1997. Remote X-ray spectrometry for NEAR and future missions: modeling and analyzing X-ray production from source to target. J. Geophys. Res. 102 (E7), 16384–16631.

Cohen, B.A., Swindle, T.D., Kring, D.A., 2005. Geochemistry and ^{40}Ar–^{39}Ar geochronology of lunar highland meteorite impact melt clasts. Meteorit. Planet. Sci. 40, 755–777.

Delano, J.W., 1986. Pristine lunar glasses: criteria, data and implications. J. Geophys. Res. 91 (D), 201–213.

Dunkin, S.K., Grande, M., Casanova, I., Fernandes, V., Heather, D.J., Kellett, B., Muinonen, K., Russell, S.S., Browning, R., Waltham, N., Parker, D., Kent, B., Perry, C.H., Swinyard, B., Perry, A., Feraday, J., Howe, C., Phillips, K., McBride, G., Huovelin, J., Muhli, P., Hakala, P.J., Vilhu, O., Thomas, N., Hughes, D., Alleyne, H., Grady, M., Lundin, R., Barabash, S., Baker, D., Clark, P.E., Murray, C.D., Guest, J., d'Uston, L.C., Maurice, S., Foing, B., Christou, A., Owen, C., Charles, P., Laukkanen, J., Koskinen, H., Kato, M., Sipila, K., Nenonen, S., Holmstrom, M., Bhandari, N., Elphic, R., Lawrence, D., 2003. Scientific rationale for the D-CIXS X-ray spectrometer on board ESA's SMART-1 mission to the Moon. Planet. Space Sci. 51, 435–442.

Fernandes, V.A., Burgess, R., Turner, G., 2000. Laser argon-40–argon-39 age studies of Dar al Gani 262 lunar meteorite. Meteorit. Planet. Sci. 35, 1355–1364.

Fernandes, V.A., Burgess, R., Turner, G., 2003. ^{40}Ar–^{39}Ar chronology of lunar meteorites NWA 032 and 773. Meteorit. Planet. Sci. 38, 555–564.

Fraser, G.W., Carpenter, J.D., Rothery, D.A., Pearson, J.F., Huovelin, J., Treis, J., Anttila, M., Ashcroft, M., Benkoff, J., Bowyer, A., Bradley, A., Bridges, J., Brown, C., Bulloch, C., Bunce, E.J., Christensen, U., Evans, M., Fairbend, R., Feasey, M., Giannini, F., Hermann, S., Hesse, M., Hilchenbach, M., Jorden, T., Joy, K., Kaipiainen, M., Kitchingman, I., Lechner, P., Lutz, G., Malkki, A., Martindale, A., Muinonen, K., Näränen, J., Portin, P., Prydderch, M., San Juan, J., Sclater, E., Schyns, E., Stevenson, T.J., Strüder, L., Syrjasuo, M., Talboys, D., Thomas, P., Whitford, C., Whitehead, S., 2008. The Mercury Imaging X-ray Spectrometer (MIXS) on BepiColombo, Planet. Space Sci., in press.

Gaddis, L.R., Hawke, B.R., Robinson, M.S., Coombs, C., 2000. Compositional analyses of small lunar pyroclastic deposits using Clementine multispectral data. J. Geophys. Res. 105 (E2), 4245–4262.

Gnos, E., Hofmann, B.A., Al-Kathiri, A., Lorenzetti, S., Eugster, O., Whitehouse, M.J., Villa, I., Jull, A.J.T., Eikenberg, J., Spettel, B., Krähenbühl, U., Franchi, I.A., Greenwood, G.C., 2004. Pinpointing the source of a lunar meteorite: implications for the evolution of the Moon. Science 305, 657–659.

Goodrich, C.A., Taylor, G.J., Keil, K., 1985. An apatite-rich, ferroan, mafic lithology from lunar meteorite ALHA81005. In: Proc. 16th Lunar Planet. Sci. Conf. J. Geophys. Res. 90, C405–C414.

Grande, M., Browning, R., Waltham, N., Parker, D., Dunkin, S.K., Kent, B., Kellett, B., Perry, C.H., Swinyard, B., Perry, A., Feraday, J., Howe, C., McBride, G., Phillips, K., Huovelin, J., Muhli, P., Hakala, P.J., Vilhu, O., Laukkanen, J., Thomas, N., Hughes, D., Alleyne, H., Grady, M., Lundin, R., Barabash, S., Baker, D., Clark, P.E., Murray, C.D., Guest, J., Casanova, I., D'Uston, L.C., Maurice, S., Foing, B., Heather, D.J., Fernandes, V., Muinonen, K., Russell, S.S., Christou, A., Owen, C., Charles, P., Koskinen, H., Kato, M., Sipila, K., Nenonen, S., Holmstrom, M., Bhandari, N., Elphic, R., Lawrence, D., 2003. The D-CIXS X-ray mapping spectrometer on SMART-1. Planet. Space Sci. 51, 427–433.

Grande, M., Kellett, B.J., Howe, C., Perry, C.H., Swinyard, B., Dunkin, S.K., Huovelin, J., Alha, L., D'Uston, L.C., Maurice, S., Gasnault, O., Couturier-Doux, S., Barabash, S., Joy, K.H., Crawford, I.A., Lawrence, D., Fernandes, V., Casanova, I., Wieczorek, M., Thomas, N., Mall, U., Foing, B., Hughes, D., Alleyne, H., Russell, S., Grady, M., Lundin, R., Baker, D., Murray, C.D., Guest, J., Christou, A., 2007. The D-CIXS X-ray spectrometer on the SMART-1 mission to the Moon—first results. Planet. Space Sci. 55, 494–502.

Grande, M., Maddison, B.J., Howe, C.J., Kellett, B.J., Swinyard, B., Sreekumar, P., Huovelin, J., Crawford, I.A., Duston, C.L., Smith, D., Cook, A., Wilding, M., Shrivastava, A., Narendranath, S., Joy, K.H., Gasnaut, O., Maurice, S., Holland, A., Rothery, D.A., Anand, M., Russell, S.S., Goswami, N., Bhandari, N., Lawrence, D., Fernandes, V.A., Wieczorek, M., Okada, T., Koschney, D., Foing, B., Pieters, C., 2009. The C1XS X-Ray Spectrometer on Chandrayaan-1, Planet. Space Sci., this issue.

Green, R.O., Pieters, C., Moroulis, P., Sellars, G., Eastwood, M., Geier, S., Shea, J., 2007. The Moon mineralogy mapper: characteristics and early laboratory calibration results. Lunar Planet. Sci. Conf. 38, 2354.

Hanser, F.A., Sellers, F.B., 1996. Design and calibration of the GOES-8 solar X-ray sensor: the XRS. SPIE Proc. 2812, 345.

Haskin, L., Warren, P., 1991. Lunar chemistry. In: Heiken, G.H., Vaniman, D., French, B.M. (Eds.), Lunar Sourcebook: A User's Guide to The Moon. Cambridge University Press, Cambridge, p. 357.

Hawke, B.R., Spudis, P.D., Clark, P.E., 1985. The origin of selected lunar geochemical anomalies: implications for early volcanism and the formation of light plains. Earth Moon Planets 32, 257–273.

Hawke, B.R., Coombs, C.R., Gaddis, L.R., Lucey, P.G., Owensby, P.D., 1989. Remote sensing and geologic studies of localized dark mantle deposits on the Moon. In: Proceedings of the 19th Lunar and Planetary Science Conference, pp. 255–268.

Head, J.W., Wilson, L., 1979. Alphonsus-type dark-halo craters: morphology, morphometry, and eruption conditions. In: Proceedings of the 10th Lunar and Planetary Science Conference, pp. 2861–2897.

Hiesinger, H., Head, J.W., Wolf, U., Jaumann, R., Neukum, G., 2003. Ages and stratigraphy of mare basalts in Oceanus Procellarum, Mare Nubium, Mare Cognitum and Mare Insularum. J. Geophys. Res. 108 (E7), 1–27.

Holland, A.D., Hutchinson, I.B., Smith, D.R., Pool, P., 2004. Photon damage in the E2V swept charge device. Nucl. Instrum. Methods Phys. Res. 521, 393–398.

Howe, C.J., Drummond, D., Edeson, R., Maddison, B., Parker, D.J., Parker, R., Shrivastava, A., Spencer, J., Kellett, B.J., Grande, M., Sreekumar, P., Huovelin, J., Smith, D.R., Gow, J., Narendranath, S., d'Uston, L., 2008a. Chandrayaan-1 X-ray spectrometer (C1XS): instrument design & technical details, Planet. Space Sci., this issue.

Howe, C.J., Edeson, E., Gow, J., 2008b. Effects of increased Earth–Moon transit time on C1XS performance, C1XS Technical Note, C1-C1X-RAL-TN-0034.

Jolliff, B.L., 2006. What is the composition of the Moon's lower crust? Lunar Planet. Sci. Conf. 37, 2346.

Jolliff, B.L., Gillis, J.J., Haskin, L.A., Korotev, R.L., Wieczorek, M.A., 2000. Major lunar crustal terranes: surface expressions and crust-mantle origins. J. Geophys. Res. 105, 4197–4216.

Jolliff, B.L., Wieczorek, M.A., Shearer, C.K., Neal, C.R. (Eds.), 2006. New Views of the Moon, Rev. Min. Geochem., Vol. 60. Mineralogical Society of America, 721pp.

Joy, K.H., 2007. Studies in lunar geology and geochemistry using sample analysis and remote sensing measurements, Ph.D. dissertation, University of London; 286pp.
Joy, K.H., Crawford, I.A., Russell, S.S., Swinyard, B., Kellett, B., Grande, M., 2006. Lunar regolith breccias MET 01210, PCA 02007 and DAG 400: their importance in understanding the lunar surface and implications for the scientific analysis of D-CIXS data. Lunar Planet. Sci. Conf. 37, 1274.
Joy, K.H., Crawford, I.A., Kellett, B., Grande, M.N., the C1XS Science Team, 2008. The scientific case for the Chandrayaan-1 X-ray spectrometer. Lunar Planet. Sci. Conf. 39, 1070.
Kellett, B.J., Narendranath, S., Sreekumar, P., Wallner, M., Maddison, B., Howe, C.J., Joy, K.H., Weider, S., Grande, M., 2008. Chandrayaan-1 X-ray spectrometer (C1XS)—instrument calibration & testing, Planet. Space Sci., submitted.
Kiran Kumar, A.S., Roy Chowdhury, A., 2005. Hyperspectral Imager in visible and near-infrared for lunar compositional mapping. J. Earth Syst. Sci. 114, 721–724.
Korotev, R.L., 2005. Lunar geochemistry as told by lunar meteorites. Chemie der Erde 65, 297–346.
Kramer, G.Y., Jolliff, B.L., Neal, C.R., 2004. Searching the Moon for aluminous mare basalts using compositional remote-sensing constraints I: finding the regions of interest. Lunar Planet. Sci. Conf. 35, 2077.
Lawrence, D.J., Feldman, W.C., Elphic, R.C., Little, R.C., Prettyman, T.H., Maurice, S., Lucey, P.G., Binder, A.B., 2002. Iron abundances on the lunar surface as measured by the Lunar Prospector gamma-ray and neutron spectrometers. J. Geophys. Res. 107 (E12), 5130.
Longhi, John, 2006. Petrogenesis of picritic mare magmas: constraints on the extent of early lunar differentiation. Geochim. Cosmochim. Acta 70, 5919–5934.
Lucey, P.G., Gillis, J.J., Steutel, D., 2004. Global images of Mg-number derived from Clementine data. Lunar Planet. Sci. Conf. 35, 1717.
Lucey, P.G., et al., 2006. Understanding the lunar surface and space–Moon interactions. In: Jolliff, B.L., et al. (Eds.), New Views of the Moon. Rev. Min. Geochem., vol. 60, pp. 83–219.
Maddison, B., Crawford, I.A., Joy, K.H., 2006. C1XS science requirements document, RAL Document: C1-C1X-RAL-RS-0003, 10pp.
Mall, U., Nathues, A., Vilenius, E., Ullaland, K., McKenna-Lawlor, S., the SIR-2 Collaboration, 2007. Sir-2 on Chandrayaan-1. Geophys. Res. Abstr. 9, 10425.
Mandel'Shtam, S.L., Tindo, I.P., Cheremukhin, G.S., Sorokin, L.S., Dmitriev, A.B., 1968. Lunar X-ray and the cosmic X-ray background measured by the lunar satellite LUNA-12. Cosmic Res. 6, 100–106.
Melosh, H.J., 1989. Impact Cratering: A Geologic Process. Oxford University Press, Oxford.
Milliken, R.E., Basu, A., 2000. A modified CIPW norm calculation of lunar mare basalts. (abstract #1427). In: 31st Annual Lunar and Planetary Science Conference.
Narendranath, S., Sreekumar, P., Kellet, B.J., Wallner, M., Howe, C., Maddison, B.J., Erd, C., Grande, M., 2008. Instrument response of the Chandrayaan-1 X-ray spectrometer (C1XS). Lunar Planet. Sci. Conf. 39, 1136.
Neal, C.R., Taylor, L.A., 1992. Petrogenesis of mare basalts: a record of lunar volcanism. Geochim. Cosmochim. Acta 56, 2177–2211.
Nittler, L.R., Starr, R.D., Lim, L., McCoy, T.J., Burbine, T.H., Reedy, R.C., Trombka, J.I., Gorenstein, P., Squyres, S.W., Boynton, W.V., McClanahan, T.P., Bhangoo, J.S., Clark, P.E., Murphy, M.E., Killen, R., 2001. X-ray fluorescence measurements of the surface elemental composition of asteroid 433 Eros. Meteorit. Planet. Sci. 36, 1673–1695.
Okada, T., Shirai, K., Yamamoto, Y., Arai, T., Ogawa, K., Hosono, K., Kato, M., 2006. X-ray fluorescence spectrometry of asteroid Itokawa by Hayabusa. Science 312, 1338–1341.
Okada, T., Shirai, K., Yamamoto, Y., Arai, T., Ogawa, K., Shiraishi, H., Iwasaki, M., Kawamura, T., Morito, H., Kato, M., the SELENE XRS Team, 2008. X-ray fluorescence experiments on the SELENE (KAGUYA) spacecraft. Lunar Planet. Sci. Conf. 39, 1960.
Papike, J.J., Ryder, G., Shearer, C.K., 1998. Lunar samples. In: Papike, J.J. (Ed.), Planetary Materials. Mineralogical Society of America, Washington, DC, pp. 5-1–5-234.
Pieters, C.M., Head, J.W., Gaddis, L., Jolliff, B.L., Duke, M., 2001. Rock types of the South Pole-Aitken basin and extent of basaltic volcanism. J. Geophys. Res. 106 (E11), 28001–28022.
Prettyman, T.H., Hagerty, J.J., Elphic, R.C., Feldman, W.C., Lawrence, D.J., McKinney, G.W., Vaniman, D.T., 2006. Elemental composition of the lunar surface: analysis of gamma ray spectroscopy data from Lunar Prospector. J. Geophys. Res. 111, E12007.
Schlemm, C.E., et al., 2007. The X-ray spectrometer on the MESSENGER spacecraft. Space Sci. Rev. 131, 393–415.
Shearer, C.K., Floss, C., 2000. In: Canup, R.M., Righter, K. (Eds.), Origin of the Earth and Moon. UAP, pp. 339–359.
Shearer, C.K., Hess, P.C., Wieczorek, M.A., Pritchard, M.E., Parmentier, E.M., Borg, L., Longhi, J., Elkins-Tanton, L.T., Neal, C.R., Antonenko, I., Canup, R.M., Halliday, A.N., Grove, T.L., Hager, B.H., Less, D.-C., Wiechert, U., 2006. Thermal and magmatic evolution of the Moon. In: Jolliff, B.L., et al. (Eds.), New Views of the Moon, Rev. Min. Geochem., vol. 60, pp. 365–518.
Shirai, K., Okada, T., Yamamoto, Y., Arai, T., Ogawa, K., Shiraishi, H., Iwasaki, M., Arakawa, M., Grande, M., Kato, M., 2008. Instrumentation and performance evaluation of the XRS on SELENE orbiter. Earth Planets Space 60, 277–281.
Snyder, G.A., Neal, C.R., Taylor, L.A., 1995. Processes involved in the formation of magnesian-suite plutonic rocks from the highlands of the Earth's Moon. J. Geophys. Res. 100, 9365–9388.
Spudis, P.D., 1993. The Geology of Multi-Ring Impact Basins. Cambridge University Press, Cambridge.
Swinyard, B.M., Joy, K.H., Kellett, B.J., Crawford, I.A., Grande, M., Howe, C.J., Gasnault, O., Fernandes, V.A., Lawrence, D.J., Russell, S.S., Wieczorek, M.A., Foing, B.H., the SMART-1 team, 2008. X-ray fluorescence observations of the Moon by SMART-1/D-CIXS and the first detection of Ti Kα from the lunar surface, Planet. Space Sci., this issue.
Takeda, H., Yamaguchi, A., Boggard, D.D., Karouji, Y., Ebihara, M., Ohtake, M., Saiki, K., Arai, T., 2006. Magnesian anorthosites and a deep crustal rock from the far side crust of the moon. Earth Planet. Sci. Lett. 247, 171–184.
Taylor, S.R., 1980. Refractory and moderately volatile element abundances in the Earth, Moon and meteorites. In: Proceedings of the 11th Lunar and Planetary Science Conference. pp. 333–348.
Taylor, S.R., 1982. Lunar and terrestrial crusts: a contrast in origin and evolution. Phys. Earth Planet. Interiors 29, 233–241.
Taylor, S.R., 1989. Growth of planetary crusts. Tectonophysics 161, 147–156.
Taylor, G.J., 2007. Two views of the Moon's composition. Planetary Science Research Discoveries. 〈http://www.psrd.hawaii.edu/April07/Moon2Views.html〉.
Taylor, S.R., Taylor, G.J., Taylor, L.A., 2006. The Moon: a Taylor perspective. Geochim. Cosmochim. Acta 70, 5904–5918.
Terada, K., Anand, M., Sokol, A.K., Bischoff, A., Sano, Y., 2007a. Cryptomare magmatism 4.35 Gyr ago recorded in lunar meteorite Kalahari 009. Nature 450, 849–852.
Terada, K., Sasaki, Y., Anand, M., Joy, K.H., Sano, Y., 2007b. Uranium–lead systematics of phosphates in lunar basaltic regolith breccia, Meteorite Hills 01210. Earth Planet. Sci. Lett. 259, 77–84.
Tompkins, S., Pieters, C.M., 1999. Mineralogy of the lunar crust: results from Clementine. Meteorit. Planet. Sci. 34, 25–41.
Treiman, A.H., Drake, M.J., 1983. Origin of lunar terrae meteorite ALHA 81005: clues from the presence of terrae clasts and a very low titanium mare basalt clast. Geophys. Res. Lett. 10, 783–786.
Vaniman, D., Dietrich, J., Taylor, G.J., Heiken, G., 1991. Exploration, samples, and recent concepts of the Moon, 1991. In: Heiken, G.H., Vaniman, D., French, B.M. (Eds.), The Lunar Sourcebook: A User's Guide to The Moon. Cambridge University Press, Cambridge.
Warren, P.H., 1986. The bulk-moon MgO/FeO ratio: a highlands perspective. In: Hartmann, W.K., Phillips, R.J., Taylor, G.J. (Eds.), The Origin of the Moon. Lunar and Planetary Institute, Houston.
Warren, P.H., 2005. New lunar meteorites: implications for composition of the global lunar surface, lunar crust, and the bulk Moon. Meteorit. Planet. Sci. 40, 477–506.
Warren, P.W., Rassmusen, K.L., 1987. Megaregolith insulation, internal temperatures, and bulk uranium content of the Moon. J. Geophys. Res. 92, 3453–3465.
Wieczorek, M.A., Phillips, R.J., 1998. Potential anomalies on a sphere: applications to the thickness of the lunar crust. J. Geophys. Res. 103, 1715–1724.
Wieczorek, M.A., Zuber, M.T., 2001. The composition and origin of the lunar crust: constraints from central peaks and crustal thickness modelling. Geophys. Res. Lett. 28, 4023–4026.
Wieczorek, M.A., Jolliff, B.L., Khan, A., Pritchard, M.E., Weiss, B.P., Williams, J.D., Hood, L.L., Righter, K., Neal, C.R., Shearer, C.K., McCallum, I.S., Tompkins, S., Hawke, B.R., Peterson, C., Gillis, J.J., Bussey, B., 2006. The constitution and structure of the lunar interior. In: Jolliff, B.L., et al. (Eds.), New Views of the Moon, Rev. Min. Geochem., vol. 60, pp. 221–364.
Wilhelms, D.E., 1987. The geologic history of the Moon, USGS Prof. Paper 1348.
Yin, L.I., Trombka, I., Adler, I., Bielefeld, M., 1993. X-ray remote sensing techniques for geochemical analysis of planetary surfaces. In: Pieters, C.M., Englert, J. (Eds.), Remote Geochemical Analysis: Elemental and Mineralogical Composition. Cambridge University Press, Cambridge, pp. 199–212.